

Detailed spectrophotometric study of the giant H II region NGC 604

Angeles I. Díaz[★] *Royal Greenwich Observatory, Herstmonceux Castle, Hailsham, East Sussex BN27 1RP and Institut d'Astrophysique, Université de Liège, Av de Cointe 5, B-4200 Cointe-Ougree, Belgium*

Elena Terlevich *Astronomy Centre, University of Sussex, Falmer, Brighton, East Sussex BN1 9QH*

B. E. J. Pagel *Royal Greenwich Observatory, Herstmonceux Castle, Hailsham, East Sussex BN27 1RP*

José M. Vilchez *Instituto de Astrofísica de Canarias, La Laguna, Tenerife, Spain*

Michael G. Edmunds *Department of Applied Mathematics and Astronomy, University College, PO Box 78, Cardiff CF1 1XL*

Accepted 1986 November 5. Received 1986 November 5; in original form 1986 July 22

Summary. Detailed spectrophotometry in the visual and near-infrared (NIR) is presented for four different slit positions over the core of NGC 604. The excitation ($[\text{O II}]/[\text{O III}]$) varies considerably both along the slit and between different slit positions, but the line ratios $([\text{O II}]+[\text{O III}])/H\beta$, $[\text{N II}]/[\text{O II}]$, $[\text{N II}]/[\text{S II}]$ and $([\text{O II}]/H\beta) \times ([\text{O II}]/[\text{S II}])$ are effectively constant, confirming the suitability of these line ratios as abundance-related parameters characterizing an entire giant H II region.

The $[\text{O III}]$ electron temperature shows significant variations across the nebula, but no significant variations in relative abundances of O, N, Ne and S are found, despite the presence of clusters of WR stars and a supernova remnant. By introducing a new ionization correction scheme we determine a helium abundance $Y=0.260\pm0.013$ and this is also constant except possibly in one place where the correction for neutral helium is very uncertain. The spectrum is consistent with ionizing stars having a representative effective temperature of 40 000 K (blanketed LTE models) or 37 000 K (non-LTE models).

1 Introduction

Giant extragalactic H II regions (GEHRs) are outstandingly large H II regions with dimensions of up to 1 kpc in some instances and a substantial number (>20) of ionizing stars. When located in

[★]Now at Departamento de Física Teórica, Universidad Autónoma de Madrid, 28049-Madrid, Spain.

nearby galaxies, they offer a unique opportunity to study the ionization structure of a giant H II complex. This is of importance for at least two reasons: (i) to find out whether consistent abundances can be derived for locations in different parts of the nebula with different degrees of ionization, and (ii) to see whether there are local abundance variations within such a complex. These variations could conceivably arise as the result of ejection of material from massive stars during the course of their evolution and would provide information about the effect of stellar mass loss and associated dynamical processes on the environment.

In order to try to shed some light on these two questions, we undertook a programme of detailed long-slit spectrophotometric observations of GEHRs which would provide good spectral and spatial resolution. In order to obtain as much spectral information as possible, we used two detectors, one sensitive to the 3500–7000 Å region (IPCS) and another to cover the 6300–9800 Å region (CCD) with the same long-slit spectrograph. The resulting 2-D spectra covered the range from [O II] $\lambda\lambda 3727, 3729$ Å to [S III] $\lambda\lambda 9069, 9532$ Å. This is the first of a series of papers reporting the results of our programme.

NGC 604 is the largest H II region in the nearby spiral galaxy M33. It is similar in some respects to the 30 Dor complex in the LMC and might be considered as one of the prototypes of a GEHR. It shows a core–halo morphology with dimensions of about 220 pc diameter for the core and 450 pc diameter for the halo (Aller 1984) and also numerous filaments similar to those found in 30 Dor (Rosa & D’Odorico 1982). According to Israel & van der Kruit (1974), NGC 604’s radio emission is predominantly thermal implying a mass of ionized gas of up to $2 \times 10^6 M_{\odot}$ and a total output of ionizing photons equal to that of 100 O6 stars. This agrees with the photon rate of $1.5 \times 10^{51} \text{ s}^{-1}$ deduced by Wooden (1983, unpublished work) for the H β luminosity of $7 \times 10^{38} \text{ erg s}^{-1}$ measured by Melnick (1979). Strong Wolf-Rayet (WR) emission features have been identified in the spectrum of NGC 604 at several locations in its core (Rosa & D’Odorico 1981; Conti & Massey 1981) thus showing the presence of very massive hot stars. The large amounts of gas and hot stars present would then qualify the nebula as a violent star formation region (VSFR, Terlevich & Melnick 1981).

Since NGC 604 is an easily observable, well-known H II region, it has received considerable attention during the last decade (e.g. Peimbert 1970; Smith 1975; Hawley & Grandi 1977; Kwitter & Aller 1981; D’Odorico, Rosa & Wampler 1983; Wooden 1983, unpublished work). Some information exists on the ionization structure of the nebula from narrow-band surface photometry (Rosa 1982) but it is far from complete. The only long-slit spectra available are the photographic plates obtained by Rosa & Solf (1984) in the restricted spectral region 6470–6790 Å, intended to provide internal kinematical information. Our observations constitute the first homogeneous set of spatially resolved spectrophotometric data over a wide spectral range, sufficient to study the ionization structure of NGC 604 and deduce the spatial distribution of the abundances of the most important elements: He, O, N, Ne and S. Somewhat similar studies have also been made of the GEHRs 30 Dor in the LMC (Mathis, Chu & Peterson 1985) and NGC 5471 in M101 (Skillman 1985). The observations are described in Section 2 of this work while the reduction of the data obtained is described in Section 3. The results are presented in Section 4 and Section 5 is devoted to their discussion and analysis. Finally, our main conclusions are summarized in Section 6.

2 Observations

NGC 604 was observed on 1984 August 19–25 with the Cassegrain spectrograph of the Isaac Newton Telescope at the Roque de los Muchachos Observatory, La Palma, Canary Islands, using the 235-mm camera and two different detectors: the Image Photon Counting System (IPCS), and

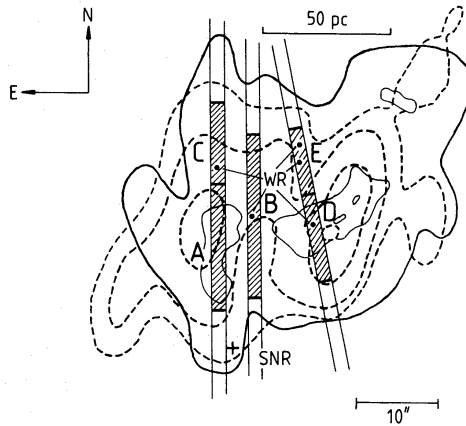


Figure 1. Sketch of NGC 604 after Rosa & D’Odorico (1982) showing the selected slit positions in our observations. The thick contours represent the [O III] distribution and dashed contours represent the 6-cm radio flux distribution. The shadowed areas labelled A, B, C, D and E represent the different regions studied in the abundance analysis. The positions of WR clusters are also indicated.

a CCD with a GEC type P8600 front-illuminated chip, using different gratings in order to cover a wide spectral region from 3500 Å to up to 1 μm.

For the IPCS observations two different gratings were used: a 300 grooves mm⁻¹ grating giving a dispersion of 137 Å mm⁻¹ over the spectral range from 3500 to 7000 Å and a blue-blazed 1200 grooves mm⁻¹ grating giving a dispersion of 35 Å mm⁻¹ in the spectral range 4200–5200 Å. With the slit width used for the observations (180 μm) the spectral resolution achieved was better than 4 Å in the first case and 1 Å in the second, the seeing varying between 1.0 and 1.2 arcsec. The data were collected in 51 spatial increments each about 1.5 arcsec long, and the spatial resolution attained was better than 3 arcsec.

The CCD used here has a physical size of 580 pixels of 22 μm squared. Therefore, in order to cover the spectral range from 6300 to 9800 Å with a linear dispersion similar to that achieved with the IPCS, i.e. 104 Å mm⁻¹, we used a red-blazed 400 lines mm⁻¹ grating and three exposures with different grating angles. These three spectra were later merged before flux calibration. The size of the CCD along the spatial direction is 400 pixels of 0.69 arcsec each.

Two different positions in the nebula were observed in the whole 3500–9800 Å spectral region. They correspond to position angles 352° and 340° (AC and DE in Fig. 1) and were chosen to match previous observations by D’Odorico *et al.* (1983, hereafter DRW83). A third position, labelled B

Table 1. Journal of observations.

Position	Night	Detector	P.A.	Grating	$\Delta\lambda$ (Å)	Exposure (sec)	Comments
AC	1984 Aug. 19/20	CCD	352°	400R	6300–7600	1000	
AC	"	"	"	400R	7400–8700	1000	
AC	"	"	"	400R	8500–9800	1500	
AC	1984 Aug. 21/22	IPCS	"	300V	3500–7400	1543	ND=0.72
AC	"	"	"	300V	3500–7400	2089	
AC	1984 Aug. 24/25	"	"	1200B	4260–5250	3000	
DE	1984 Aug. 19/20	CCD	340°	400R	6300–7600	500	
DE	"	"	"	400R	7400–8700	500	
DE	"	"	"	400R	8500–9800	1000	
DE	1984 Aug. 21/22	IPCS	"	300V	3500–7400	1505	ND=0.72
DE	"	"	"	300V	3500–7400	2001	
DE	1984 Aug. 24/25	"	"	1200B	4260–5260	2040	
B	1984 Aug. 21/22	"	352°	300V	3500–7400	2009	
B	1984 Aug. 22/23	"	"	300V	3500–7400	1003	ND=0.72

in the figure, intermediate between A and D, at position angle 352°, was observed only in the 3500–7000 Å region of the spectrum. All observations in this region were made with and without an appropriate neutral density filter in order to avoid the effects of saturation in the strongest lines in the first case and to obtain good signal-to-noise for the weak lines in the second. A journal of observations is presented in Table 1.

3 Reductions

The reduction of the data was carried out at the STARLINK node at RGO using standard software packages. We followed a 2-D reduction procedure as much as possible in order to exploit the available spatial information. The IPCS frames were wavelength calibrated, sky subtracted, extinction corrected and flux calibrated in two dimensions. In the case of the CCD observations, the large number of spatial elements involved made this entire 2-D procedure too time consuming and it was abandoned after wavelength calibration. Prior to that, subtraction of pre-flash frames (needed for this particular CCD) and of a dark current bias were performed, as well as the removal of typically 30 cosmic ray events per frame, due to the long exposure times involved. The subsequent steps in the reduction procedure, i.e. sky subtraction, extinction correction and flux calibration, were then accomplished for selected sets of increments compressed to one dimension. These increments were chosen on the basis of the spatial light variation along the slit (see Fig. 2).

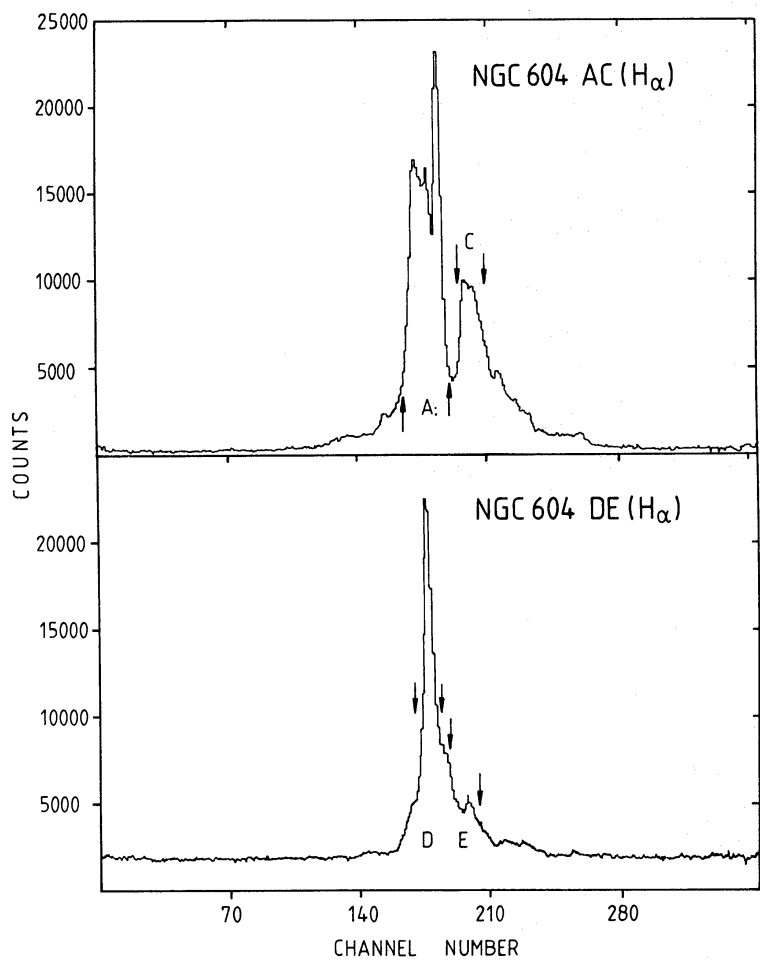


Figure 2. Spatial profile of H α extracted from the CCD observations. The arrows mark the regions selected along the slit, and the ordinates give counts over the whole line profile per spatial increment.

Wavelength calibrations in all cases were accurate to better than 1 Å. With regard to the background subtraction procedure, the nebula appeared sufficiently extended to fill up the slit almost entirely and therefore the sky subtraction was made using the outermost increments in every data frame. This procedure proved to be good as evidenced by the inspection of the reduced spectra in the sky [O I] line regions at $\lambda\lambda 5577$, 6300 and 6364 Å and the total absence of sky features in the red (7000–9800 Å), a spectral region particularly crowded with sky lines.

The spectra were corrected for continuous atmospheric extinction using an extinction curve appropriate for the La Palma Observatory (LPO). The atmospheric absorption bands (mainly O₂ and water vapour) present in the red part of the spectrum (see Díaz, Pagel & Wilson 1985) had to be removed by means of division by the standard star HR 7596. However, narrow saturated water vapour lines are not successfully eliminated in this way and, in some cases, can seriously affect the measurements of the [S III] lines (mainly at $\lambda 9532$ Å) as will be discussed in the following section.

Finally, the flux calibration was achieved by comparison with selected standard star observations: L1363–3 (Oke 1974) and BD+404032 (Stone 1977) for the 3500–7500 Å region and HR 7596 (Hayes 1970) for the 6300–9800 Å region.

4 Results

Fig. 2 shows the spatial distribution of the H α flux from south to north along the slit, for the two positions in the nebula that were observed in the whole spectral range 3500–9800 Å. This figure offers a first insight into the fine structure of the nebula and was used as a base for defining the regions from where the spectra were to be extracted. These regions are also indicated in Fig. 1.

Fig. 3 shows the low-resolution merged spectra for four different locations in the nebula. The weaker lines were easily detected and measured in the high-resolution spectra as can be seen from Fig. 4. No WR features are seen at position A. B and C show the broad feature at $\lambda 4650$ Å characteristic of WN stars. E contains both WN and WC stars as evidenced by the presence of the broad features at $\lambda 4100$ Å (C IV + He II), $\lambda 4650$ Å (C III + C IV) and $\lambda 5800$ Å (C IV). Our spectra of position D show only the barest trace of a broad feature at $\lambda 4650$ Å.

4.1 LINE INTENSITIES

Line intensity ratios for the most relevant emission lines were measured in each spectrum using the program LINES (kindly made available to us by Roberto Terlevich and Jack Baldwin), which integrates each line between chosen limits and a fitted continuum, and were weighted according to their signal-to-noise ratio when more than one spectrum was used. They are listed in Tables 2 and 3 for the IPCS and CCD data, respectively. The errors quoted in Table 2 were obtained from photon statistics analysis and do not include any error regarding the continuum placement, which did not present any difficulty. Our results are in satisfactory agreement with the limited data given by DRW83 for the same regions. For the CCD spectra an additional source of error was introduced by the correction for atmospheric absorption; this error affects more severely the red end of the spectrum and estimated values are given in Table 3. The final column in Table 3 represents the straight sum of the photon counts in the four slit positions.

The negative radial velocity of NGC 604 (-238 km s^{-1} ; de Vaucouleurs & de Vaucouleurs 1971) shifts the [S III] $\lambda 9532$ Å line towards the water vapour bands. Hence our atmospheric absorption correction procedure does not successfully eliminate the effect of narrow saturated lines, in the fluxes of $\lambda 9532$ Å. However, the $\lambda 9069$ Å line seems to be free of absorption effects. Due to the velocity field through the nebula (see for example Rosa & D’Odorico 1982) this effect is not the same for every spectrum, being stronger for location A and almost negligible for location E.

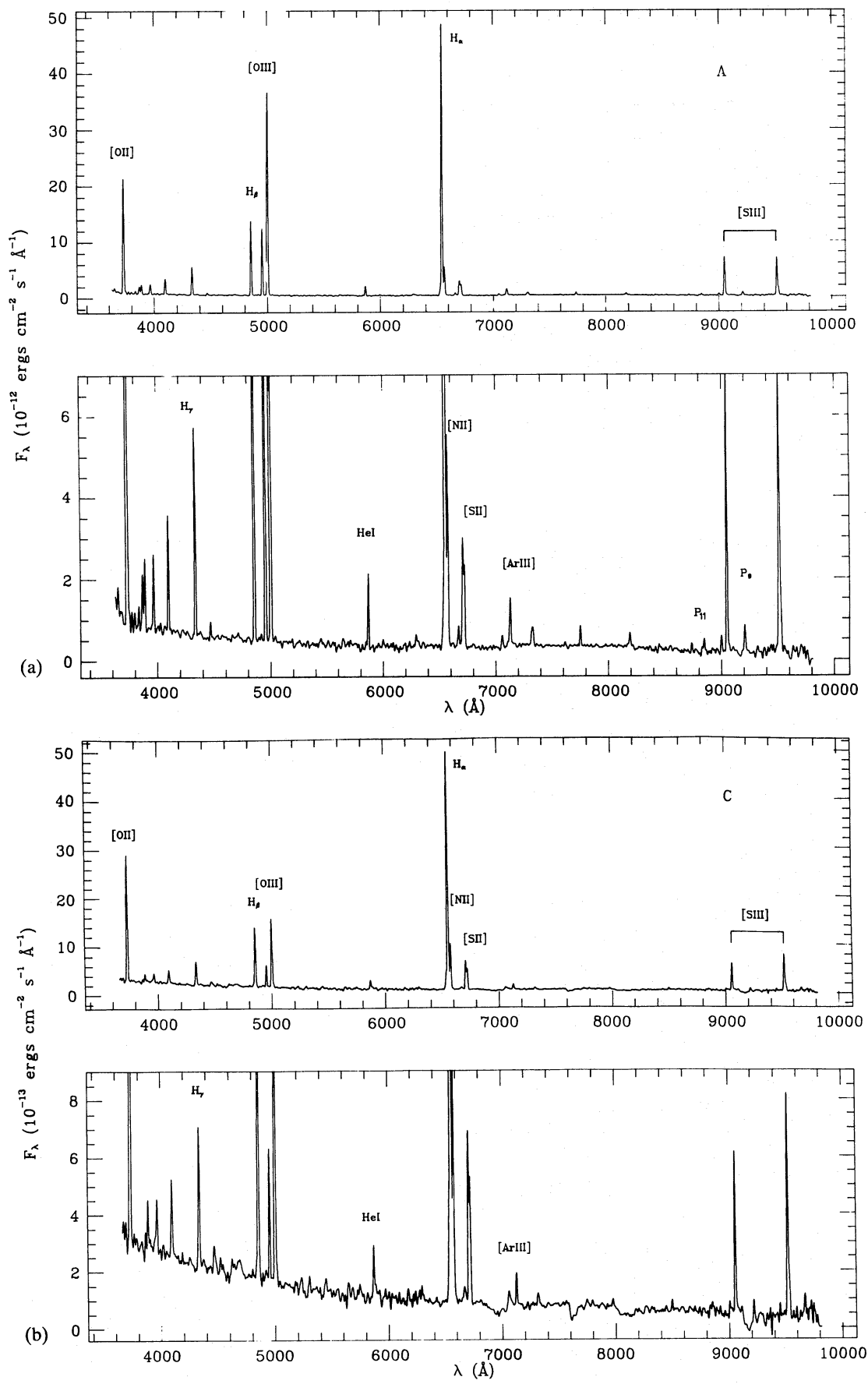


Figure 3. Merged low-resolution spectra for regions A, C, D and E. The IPCS and CCD spectra were merged at H α . Note the broad features due to the underlying WR clusters (particularly prominent in position E) and the effects of atmospheric absorption on [S III] 49532 Å.

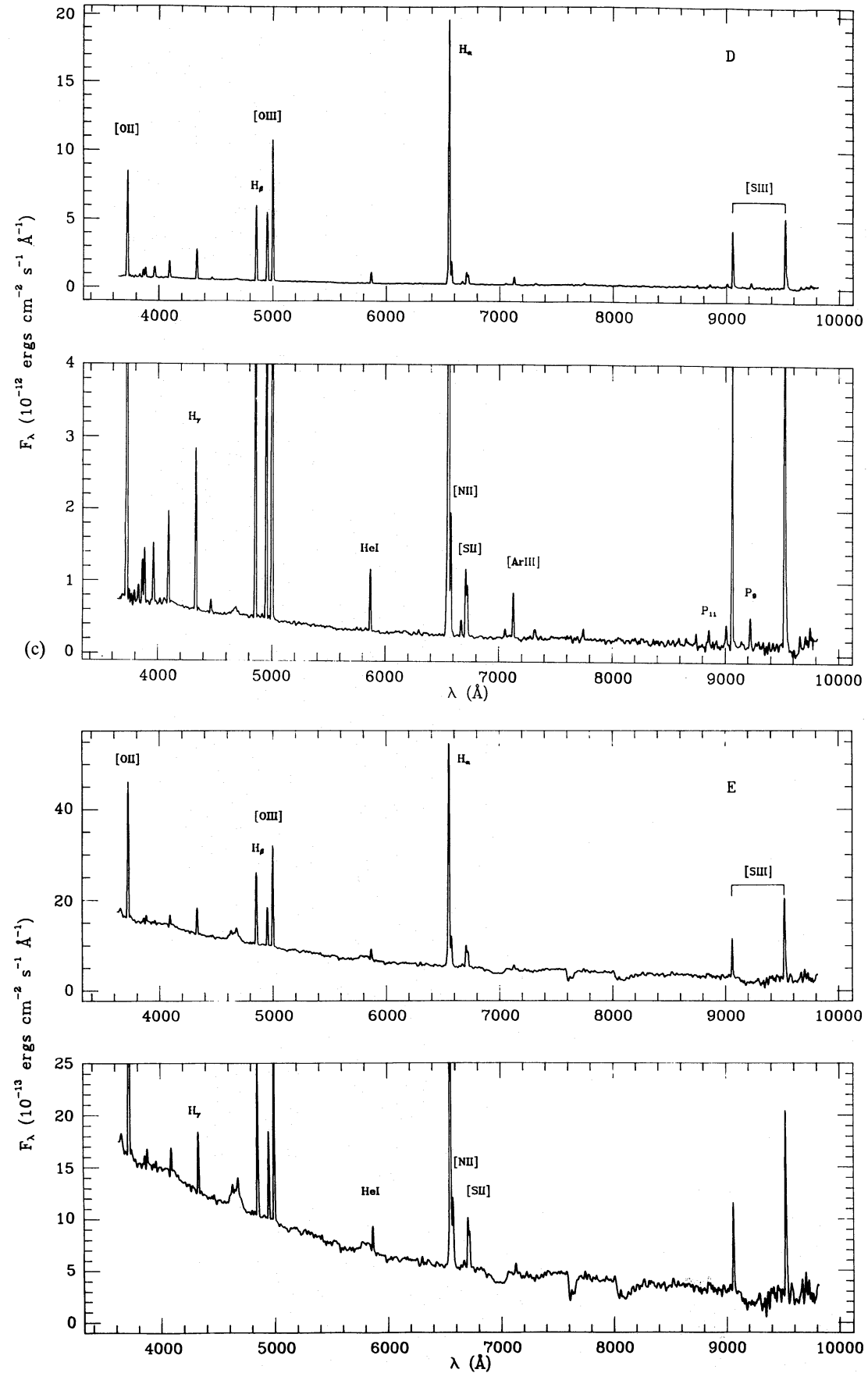


Figure 3-continued

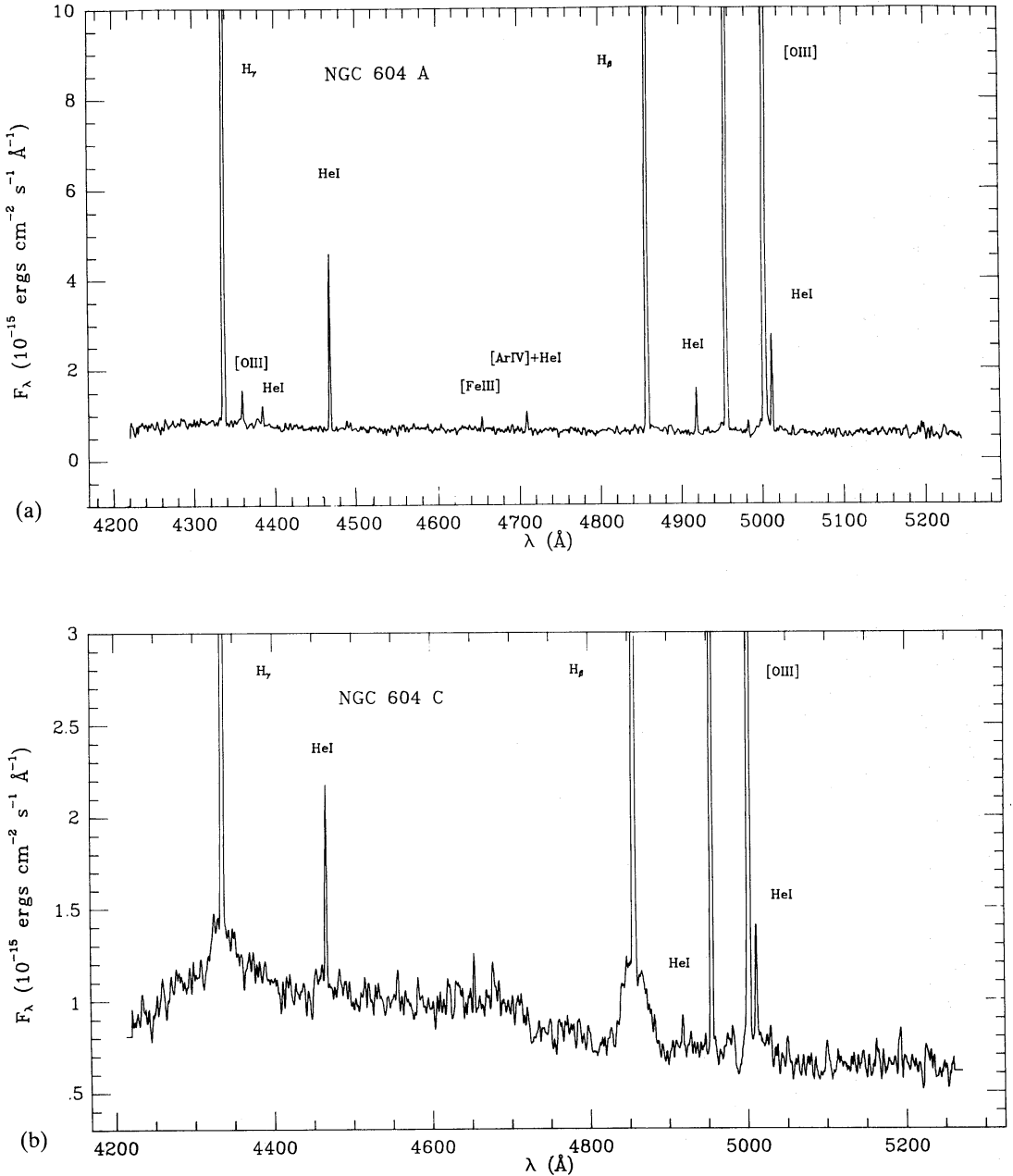


Figure 4. (a) Example of IPCS high-resolution spectrum at position A. The significant lines are shown in the figure. (b) High-resolution IPCS spectrum at position C; notice the striking broad components. The broad component in $\text{H}\beta$ contributes by 1/5 to the total flux in the line.

The observed line-intensity ratios were corrected for reddening according to a standard reddening curve (Whitford 1958) and assuming the theoretical values for the Balmer decrements corresponding to case B recombination (Brocklehurst 1971). The three ratios $\text{H}\alpha/\text{H}\beta$, $\text{H}\gamma/\text{H}\beta$ and $\text{H}\delta/\text{H}\beta$ were used weighted by their corresponding baseline in $1/\lambda$ and signal-to-noise. The reddening constant $C(\text{H}\beta)$ thus deduced is given in Table 2 for each location.

In the two positions where the stellar continuum is stronger, underlying absorption seems to be present slightly affecting the Balmer decrements. An assumed equivalent width for the Balmer absorption lines of 1.2 \AA , found by means of an iterative process (McCall, Rybski & Shields

Table 2. Reddening-corrected line intensity ratios from IPCS observations for the regions showed in Fig. 1, referred to $H\beta=100$. Balmer lines are also corrected for 1.2 Å underlying absorption. The reddening coefficient, $C(H\beta)$, the measured $H\beta$ flux [$I_0(H\beta)$] and $H\beta$ and $H\delta$ equivalent width [EW($H\beta$) and EW($H\delta$)] are also listed. The reddening-corrected flux in $H\beta$ refers to the entire region illustrated in Fig. 1. An integrated spectrum is presented in column Σ . Broad WR features are observed at some positions, as can be seen in Fig. 3, in agreement with previous work by DRW83.

REGION			A	C	D	E	B	Σ
LINE	ION	$f(\lambda)$						
3727 [OII]		0.26	208.0 \pm 2.5	248.7 \pm 4.3	161.4 \pm 2.0	257.0 \pm 2.5	200.0 \pm 2.0	215.2 \pm 1.1
3750 H12		0.2			4.3 \pm 0.9		2.2 \pm 0.4	5.8 \pm 0.4
3770 H11		0.26			3.4 \pm 0.7		2.2 \pm 0.4	
3797 H10		0.25	3.6 \pm 0.5	4.7 \pm 0.7	4.3 \pm 0.3		5.3 \pm 0.7	
3835 H9		0.24	6.0 \pm 0.5	4.7 \pm 0.4	5.9 \pm 0.4		5.4 \pm 0.5	
3869 [NeIII]		0.23	15.5 \pm 1.1	2.6 \pm 0.2	12.6 \pm 0.4	8.9 \pm 0.4	6.9 \pm 0.6	10.8 \pm 0.2
3889 H8, HeI		0.22	17.4 \pm 1.2	23.6 \pm 1.6	15.3 \pm 0.4	14.1 \pm 0.4	18.2 \pm 0.6	15.8 \pm 0.2
3969 [NeIII], H ϵ		0.21	20.0 \pm 1.6	18.8 \pm 1.3	17.5 \pm 1.3	8.9 \pm 0.2	18.6 \pm 0.7	17.5 \pm 0.2
4101 H δ		0.18	26.3 \pm 0.5	29.5 \pm 0.6	24.8 \pm 0.5	18.2 \pm 0.5 ^(*)	25.7 \pm 0.5	25.0 \pm 0.2
4340 H γ		0.135	45.7 \pm 0.8	45.1 \pm 1.0	41.7 \pm 0.8	42.7 \pm 1.1	46.8 \pm 0.9	44.3 \pm 0.4
4363 [OIII]		0.13	0.63:	<0.4	0.70 \pm 0.15		0.63 \pm 0.10	0.75 \pm 0.1
4363 (HR)*			0.62 \pm 0.06	<0.3	0.87 \pm 0.09	1.05 \pm 0.15		0.52 \pm 0.02
4471 HeI		0.10	4.2 \pm 0.6	7.2 \pm 2.3 ^(*)	3.4 \pm 2.0	3.5 \pm 1.5	3.9 \pm 0.6	3.7 \pm 0.4
4471 (HR)*			4.17 \pm 0.4	3.25 \pm 0.9	3.9 \pm 0.4	3.98 \pm 0.5		3.7 \pm 0.1
4861 H δ		0.00	100.0 \pm 1.0	100.0 \pm 1.0	100.0 \pm 1.0	100.0 \pm 1.0	100.0 \pm 1.0	100.0 \pm 0.4
4959 [OIII]		-0.02	89.1 \pm 3.5	33.3 \pm 1.0	85.1 \pm 2.5	53.5 \pm 1.3	60.3 \pm 1.8	77.5 \pm 0.7
5007 [OIII]		-0.03	269.2 \pm 2.7	97.3 \pm 1.0		151.4 \pm 2.0		207.7 \pm 0.8
5016 HeI, (HR)*			2.46 \pm 0.3	2.3 \pm 0.6	2.69 \pm 0.4	2.0 \pm 0.5 ^(*)		1.9 \pm 0.1
5876 HeI		-0.23	12.3 \pm 0.4	11.2 \pm 2.2 ^(*)	12.1 \pm 0.3	15.3 \pm 0.9 ^(*)	11.7 \pm 0.3	11.5 \pm 0.2
6300 [OI]		-0.30	1.5 \pm 0.8		1.0 \pm 0.5	2.0 \pm 1.0	2.0 \pm 1.0	
6312 [SIII]		-0.30	1.3:		0.9 \pm 0.4	1.1 \pm 0.4	1.0:	
6548 [NII]		-0.34	9.8 \pm 0.6	17.5 \pm 2.0	9.1 \pm 0.3	13.2 \pm 2.0	11.0 \pm 0.3	12.4 \pm 0.2
6563 H α		-0.34	282.0 \pm 3.1	290.0 \pm 1.9	281.0 \pm 1.4	282.0 \pm 2.5	282.0 \pm 1.2	286.0 \pm 0.8
6584 [NII]		-0.34	30.0 \pm 0.6	50.8 \pm 1.9	27.4 \pm 0.8	36.3 \pm 2.0	30.9 \pm 0.9	33.5 \pm 0.4
6678 HeI		-0.35	3.1 \pm 0.5	4.7 \pm 2.6	4.0 \pm 0.7	3.3 \pm 1.5	3.2:	2.7 \pm 0.4
6717 [SII]		-0.36	14.2 \pm 1.3	31.0 \pm 3.0	15.6 \pm 0.6	26.0 \pm 2.4	16.2 \pm 0.8	16.6 \pm 0.4
6731 [SII]		-0.36	10.7 \pm 1.5	23.0 \pm 2.2	11.1 \pm 0.5	16.4 \pm 2.3	12.9 \pm 0.6	11.8 \pm 0.4
7065 HeI		-0.40	1.8 \pm 0.5		1.2 \pm 0.2		1.2:	
7135 [ArIII]		-0.41	6.8 \pm 2.0	4.0 \pm 2.0	5.9 \pm 0.9	6.0 \pm 2.0	4.4 \pm 1.0	5.5 \pm 0.6
C($H\alpha$)			0.45	0.40	0.30	0.35	0.30	0.36
$I_0(H\alpha)$ * 10^{-13} erg cm $^{-2}$ s $^{-1}$			3.64	1.08	2.64	0.41	1.99	7.33
EW($H\alpha$) (Å)			315	90	135	18	162	86
EW($H\delta$) (Å)			42	13	19	2	25	14
WR type				-	WN	(WC)	WN+WC	WN

(*): HR indicates fluxes from high resolution data.

(*): Narrow component of lines presenting broad base and wings.

(+): Resolved from the broad CIV λ 5800 feature in the underlying stellar spectrum.

1985), provided an excellent correction. The corrected intensities are quoted in Table 2. In most cases agreement is obtained when comparing the theoretical prediction for the ratios of Paschen lines to $H\alpha$ and the observed ones after this reddening correction.

4.2 GAS DENSITIES AND TEMPERATURES

Gas densities were obtained from the ratio of the [S II] lines at $\lambda\lambda$ 6717, 6731 Å following standard procedures (see for example Aller 1984). Densities were found to be of the order of 100 cm $^{-3}$ in all cases, which corresponds to the low-density limit.

Two line ratios were used for temperature determinations: [O III] $\lambda\lambda$ 4363/ $\lambda\lambda$ 4959, 5007 Å and [O II] $\lambda\lambda$ 7320, 7330/ $\lambda\lambda$ 3727, 3729 Å. They were used according to the schemes proposed by

Table 3. Reddening-corrected line intensity ratios from the CCD observations referred to $H\alpha=286$. The reddening correction was performed using the coefficients derived for the optical data. The values for $i(\lambda)$ are the theoretical prediction for case B recombination for $H\alpha$ and the Paschen lines. Column Σ shows the fluxes for the integrated spectrum of NGC 604.

REGION				A	C	D	E	Σ
LINE	ION	$i(\lambda)$	$f(H\alpha)-f(\lambda)$					
6563	$H\alpha$		0.00	286.0 \pm 1.0	286.0 \pm 1.0	286.0 \pm 1.0	286.0 \pm 1.0	286.0 \pm 0.7
6584	[NII]		0.00	35.4 \pm 0.9	55.6 \pm 1.4	23.1 \pm 0.8	41.2 \pm 0.7	35.8 \pm 0.2
6678	HeI		0.01	3.2 \pm 0.5	4.6 \pm 0.8	3.2 \pm 0.5	3.6 \pm 0.6	3.4 \pm 0.1
6717	[SII]		0.02	16.3 \pm 1.0	34.5 \pm 1.8	12.8 \pm 0.7	28.6 \pm 1.2	20.5 \pm 0.1
6731	[SII]		0.02	14.7 \pm 1.3	25.2 \pm 1.0	10.6 \pm 0.8	22.7 \pm 1.7	16.6 \pm 0.1
7065	HeI		0.06	2.4 \pm 0.7	2.5 \pm 0.6	1.8 \pm 0.4		1.9 \pm 0.1
7135	[ArIII]		0.07	10.3 \pm 1.7	7.3 \pm 1.1	9.5 \pm 1.3	5.8 \pm 1.0	9.2 \pm 0.4
7325	[OII]		0.09	4.4 \pm 0.4	4.3 \pm 0.9	2.7 \pm 0.3		3.4 \pm 0.2
8598	P14	0.70	0.22	0.4 \pm 0.3		1.0 \pm 0.3		
8665	P13	0.82	0.24			0.9 \pm 0.3		
8750	P12	1.11	0.25	1.0 \pm 0.2		1.8 \pm 0.7		1.4 \pm 0.3
8863	P11	1.37	0.26	1.6 \pm 0.4		2.6 \pm 0.7		2.3 \pm 0.3
9015	P10	1.85	0.28	1.9 \pm 0.3	1.62:	3.8 \pm 1.0		2.7 \pm 0.3
9069	[SIII]		0.30	33.4 \pm 0.4	25.5 \pm 0.3	50.5 \pm 1.0	40.0 \pm 2.5	39.8 \pm 0.2
9229	P9	2.55	0.30	3.0 \pm 0.5	2.3 \pm 1.0	5.1 \pm 1.4		2.7 \pm 0.4
9532	[SIII]		0.31	41.0 \pm 1.6	44.3 \pm 2.2	73.0 \pm 1.5	87.5 \pm 4.4	47.6 \pm 0.5

Seaton (1975) and Aller (1984) and using the most recent atomic data in the literature (Mendoza 1983). The temperatures thus deduced are listed in Table 4 for each location in the nebula together with the mean adopted $t[O\ II]$ and $t[O\ III]$. Although the $[S\ III]\ \lambda 6312\ \text{\AA}$ is too noisy to determine a reliable value of $t[S\ III]$ the values obtained are consistent with $t[O\ II]$ and $t[O\ III]$.

4.3 IONIC ABUNDANCES

Ionic abundances of the most important elements: He, O, N, S and Ne were calculated from their corresponding measured line-intensity ratios and the adopted temperature, following a three-level atom calculation and using Mendoza’s (1983) atomic data.

For the higher states of ionization the adopted $[O\ III]$ temperature, $t[O\ III]$, was used in all cases, while the adopted $[O\ II]$ temperature, $t[O\ II]$, was used for the lower ionization states. In general the measured $t_r[O\ II]$ is found to be substantially higher than $t_r[O\ III]$, an effect which is in qualitative agreement with theoretical models by Stasinska (1980, hereafter S80), but is larger than predicted. The calculated ionic abundances are also tabulated in Table 4.

4.4 TOTAL ABUNDANCES

4.4.1 Heavy elements

Total abundances for O and N were calculated following the standard ionization scheme (Seaton 1975):

$$\frac{O}{H} = \frac{O^+ + O^{++}}{H^+},$$

$$\frac{N}{O} = \frac{N^+}{O^+}.$$

For Ne, the ratio $x(Ne^{++})/x(O^{++})$, often taken to be close to 1, is sensitive to stellar effective

Table 4. Ionic and total abundances derived from our observations and previous work in the literature. The [OII] line temperature t_r ([OII]), comes from Stasinska (1980) models; t_r temperatures are derived from the observed line ratios and the 'adopted temperatures' are the ones used for the abundance analysis. The density parameter x ([SII]) is also listed. * refers to high-dispersion data.

Temperatures and Abundances.									
	KA81	S75	PS70	A	C	D	E	B	Σ
$\log(OII+OIII)/H\beta$	0.73	0.66	0.73	0.75	0.58	0.70	0.66	0.64	0.70
t_r [OIII]	1.11	0.90	0.94	0.77	<0.82	0.85 ± 0.02	1.0 ± 0.07	0.85 ± 0.07	0.77 ± 0.01
x ([SII])	0.00			0.02	0.01	0.01	0.01	0.02	0.01
t_r [OII]	0.86			1.05 ± 0.05	1.0 ± 0.09	0.96 ± 0.08			0.94 ± 0.03
t_L [OII] Predicted	1.0:	0.9:	0.97:	0.85:		0.88	1.0	0.87	
t_r [SIII]				0.90:		0.70:	0.83 ± 0.09		
Adopted temperatures									
t [OIII]	1.11	0.90	0.94	0.77	0.8:	0.85	1.00	0.85	0.77
t [OII]	0.89	0.90	0.94	0.95	0.9:	0.88	1.00	0.87	0.94
$12+\log O^{++}/H^{+}$	7.72	8.03	7.94	8.40 ± 0.04	7.91:	8.20 ± 0.14	7.74 ± 0.08	8.05 ± 0.11	8.34 ± 0.02
$12+\log O^{+}/H^{+}$	8.21	8.04	8.09	8.00 ± 0.08	8.19:	8.03 ± 0.03	7.98 ± 0.11	8.15 ± 0.14	8.02 ± 0.06
$12+\log O/H$	8.33	8.34	8.32	8.54 ± 0.06	8.37:	8.42 ± 0.07	8.19 ± 0.11	8.40 ± 0.14	8.51 ± 0.03
$\log O^{+}/N^{+}$	1.35	1.09		1.19 ± 0.07	1.06 ± 0.10	1.17 ± 0.08	1.14 ± 0.10	1.22 ± 0.09	1.16 ± 0.04
$He^{+}/H^{+} \times 10^2$ (4471)				8.2 ± 1.2	14.2 ± 4.7	7.7 ± 0.4	8.1 ± 3.5	7.8 ± 1.1	7.3 ± 0.8
$He^{+}/H^{+} \times 10^2$ (5876)				8.6 ± 0.8	7.8 ± 1.4	8.5 ± 0.3	11.2 ± 0.8	8.3 ± 0.8	8.1 ± 0.3
$He^{+}/H^{+} \times 10^2$ (6678)				7.0 ± 1.2	10.7 ± 5.9	9.3 ± 1.7	7.8 ± 3.4	7.3 ± 0.8	6.2 ± 1.0
$He^{+}/H^{+} \times 10^2$ (4471) (*)				8.2 ± 0.7	6.5 ± 2.0	7.8 ± 0.6	8.1 ± 1.0		7.3 ± 0.2
$\langle He^{+}/H^{+} \rangle \times 10^2$	7.8	7.6	9.4	8.2 ± 0.5	7.9 ± 1.1	8.2 ± 0.2	9.9 ± 0.6	7.8 ± 0.5	7.5 ± 0.2
I C F	1.29	1.5	1.37	1.06	1.11	1.10		1.13	1.11
$He/H \times 10^2$	10.0	13.0	12.9	8.7 ± 0.6	8.6 ± 1.0	9.1 ± 0.2		8.8 ± 0.6	8.3 ± 0.3
$12+\log S^{+}/H^{+}$	5.82	5.86		5.82 ± 0.10	6.20 ± 0.10	5.94 ± 0.09	5.99 ± 0.11	5.98 ± 0.12	5.87 ± 0.05
$12+\log S^{++}/H^{+}$	6.58			6.83 ± 0.04	$6.68\pm$	6.90 ± 0.04	6.81 ± 0.11	$6.70\pm$	6.91 ± 0.03
$12+\log S/H$	6.65			6.87 ± 0.05	$6.80\pm$	6.95 ± 0.04	6.87 ± 0.10	$6.78\pm$	6.95 ± 0.03
$\log O^{++}/Ne^{++}$				0.70 ± 0.05	$1.06\pm$	0.79 ± 0.03	0.79 ± 0.09	0.90 ± 0.08	0.78 ± 0.02

temperature and modelling assumptions (*cf.* S80; Garnett & Shields 1986) and we content ourselves with quoting the ionic abundance ratio O^{++}/Ne^{++} which is probably an upper limit to O/Ne . In the case of S, total abundances were calculated from S^+ and S^{++} abundances assuming that no higher ionization states are significantly present. This is expected on the basis of theoretical models (Mathis 1982) which predict a percentage of $S^{3+}+S^{4+}/S$ between 0.05 and 0.15 for the excitation conditions of our observed regions. Also the results obtained for the Magellanic Clouds and the Orion Nebula seem to indicate that a plausible ionization scheme for S is:

$$\frac{S}{H} \sim \frac{S^+ + S^{++}}{H^+}$$

(Pagel 1978; Barker 1978; Dinerstein 1980). Therefore we have adopted this scheme for the total S abundance calculation. Abundances are given in Table 4.

4.4.2 He abundances and stellar effective temperatures

Several He I recombination lines have been detected and measured, some of which might be affected by underlying absorption, given the hot stellar population known to be present. The He^+/H^+ abundance ratio was calculated from the He I lines $\lambda\lambda 4471$, 5876 and 6678 Å by a weighted average of the values deduced from each of them. The strongest line at $\lambda 5876$ Å is probably the least affected by underlying absorption and, due to the blueshift of NGC 604, it is also free from contamination by galactic NaD absorption at $\lambda 5890$ Å. These facts make this line the most important one for the He abundance determination.

Nebular He II lines were not detected* implying that the He must be mainly in neutral and once ionized form; hence

$$\frac{He}{H} = \frac{He^0 + He^+}{H^+}.$$

The correction for the presence of neutral helium constitutes a serious problem. Different empirical methods have been proposed by different authors (e.g. Peimbert & Costero 1969; Peimbert, Rodríguez & Torres-Peimbert 1974; Lequeux *et al.* 1979) in relation to specific observations of an object or a collection of objects (e.g. Orion Nebula in the case of Peimbert & Costero 1969; blue dwarf galaxies in the case of Lequeux *et al.* 1979) but the correction is not thought to be accurate. Model calculations by S80, Mathis (1982), Rubin (1986) and Dinerstein & Shields (1986) show that in a simple geometry the He^+ and H^+ Strömgren spheres coincide within a few per cent for effective temperatures upwards of 37 500 K (NLTE models) or 40 000 K (blanketed LTE models) implying very small, if any, ionization correction factors (ICFs). For lower effective temperatures the relative size of the He zone drops sharply and the ICF becomes non-negligible and uncertain. A proper determination of the mean effective temperature of the ionizing cluster is therefore needed.

One possible method to determine this effective temperature is the one proposed by Mathis (1982, 1985). His H II region models are parametrized by a single parameter, q , analogous to the more commonly used ionization parameter, u . A family of models with different values of q describes a curve on the O^+/O versus $\log(S^{++}/S^+)$ plane, the position along the curve depending on the photon flux of the ionizing stars when the density and the filling factor are fixed. Applying this method in the low-density limit we obtain a stellar effective temperature of about 40 000 K if

*The He II line at $\lambda 4686$ Å which appears in some of the spectra, is stellar in origin, belonging to the WR stars present.

the LTE models of Kurucz (1979) are used. This temperature is intermediate between the cooler one ($\sim 35\,000$ K) found for the Orion nebula and the hotter one ($\sim 50\,000$ K) estimated for 30 Dor (which could be a younger object) and the H II regions in M101 (Mathis 1982).

An alternative method is the one proposed by S80, who uses a diagram involving the $[\text{O III}]\lambda\lambda(4363/5007)$ ratio and the oxygen abundance, as well as the predicted loci for different input stellar spectra, taken in this case from the NLTE model atmospheres of Mihalas (1972). Our values for O/H and electron temperature in NGC 604 are best fitted by a mean effective temperature of $37\,000$ K (possibly slightly lower for regions E and C).

The temperatures deduced by both methods are in fair agreement with each other and on the borderline where the ICFs become important. We have determined the ICFs for each of our regions from Stasinska's (1980, 1982) low density ($N_e=100\text{ cm}^{-3}$) homogeneous (i.e. with no density discontinuities) models, using the inverse excitation parameter

$$\eta = (\text{O}^+/\text{O}^{++})/(\text{S}^+/\text{S}^{++}).$$

We have chosen this parameter instead of the customary O^+/O^{++} one because, while this latter ratio is closely related to the ionization parameter u (which in turn depends on the number of Lyman photons, the electron density and the geometry of the region), our parameter is mostly related to the actual hardness of the radiation field which determines the ionization structure of helium, and depends much more weakly on the rest of the variables entering the models.

A one-to-one relationship holds for the predicted ICF for He^+/H^+ and the values of $\log(\eta)$ as computed from the models except for values of $\log(\eta)$ around 0.95 where the curve becomes very steep and the ICF is undefined (Vilchez, in preparation). This point of discontinuity possibly reflects the abrupt drop in the number of He ionizing photons predicted by the model atmospheres used by Stasinska (Mihalas 1972) around an effective temperature of $35\,000$ K.

Using the observed $\log(\eta)$ we obtained by interpolation the ICFs given in Table 4. No value of the ICF is given for region E where η is close to the discontinuity point in the η versus ICF relation.

5 Discussion

5.1 SPATIAL STUDY

Fig. 5 shows the spatial behaviour of the observed $[\text{O II}]/[\text{O III}]$ and $[\text{N II}]/[\text{O II}]$ line ratios for the different long-slit positions used. The ratio $[\text{N II}]/[\text{O II}]$ has been multiplied by that of $\text{H}\beta/\text{H}\alpha$ in order to reduce the effect of reddening. The Balmer decrement itself, $\text{H}\alpha/\text{H}\beta$, divided by 10 for better scaling of the figure, has also been plotted for each position observed. Its comparison with the theoretical value for case B recombination, 2.86, gives a direct indication of the reddening variation along the slit. In the $[\text{N II}]/[\text{O II}]$ plot, each spatial profile has been displaced from the preceding one by adding a constant value of 0.1.

The reddening seems remarkably constant across the nebula in the observed positions, but the excitation varies by large factors in each case, the most extreme changes appearing in position AC. C is the lowest excitation region observed as can be seen in Fig. 3. WN features are present superimposed on a relatively strong continuum, in agreement with what is found by DRW83. This region seems to coincide with a very large gas bubble surrounding a stellar-like source reported by Rosa & Solf (1984). At the other extreme, A is a high excitation almost point-like source, coincident with a sharp maximum in $[\text{O III}]$ emission reported by Rosa (1982). Neither a strong continuum nor indication of WR features can be seen in its spectrum.

Changes in excitation are also observed in the other two slit positions although smoother, with the more excited region always displaced to the south of the nebula, as is also the case for position

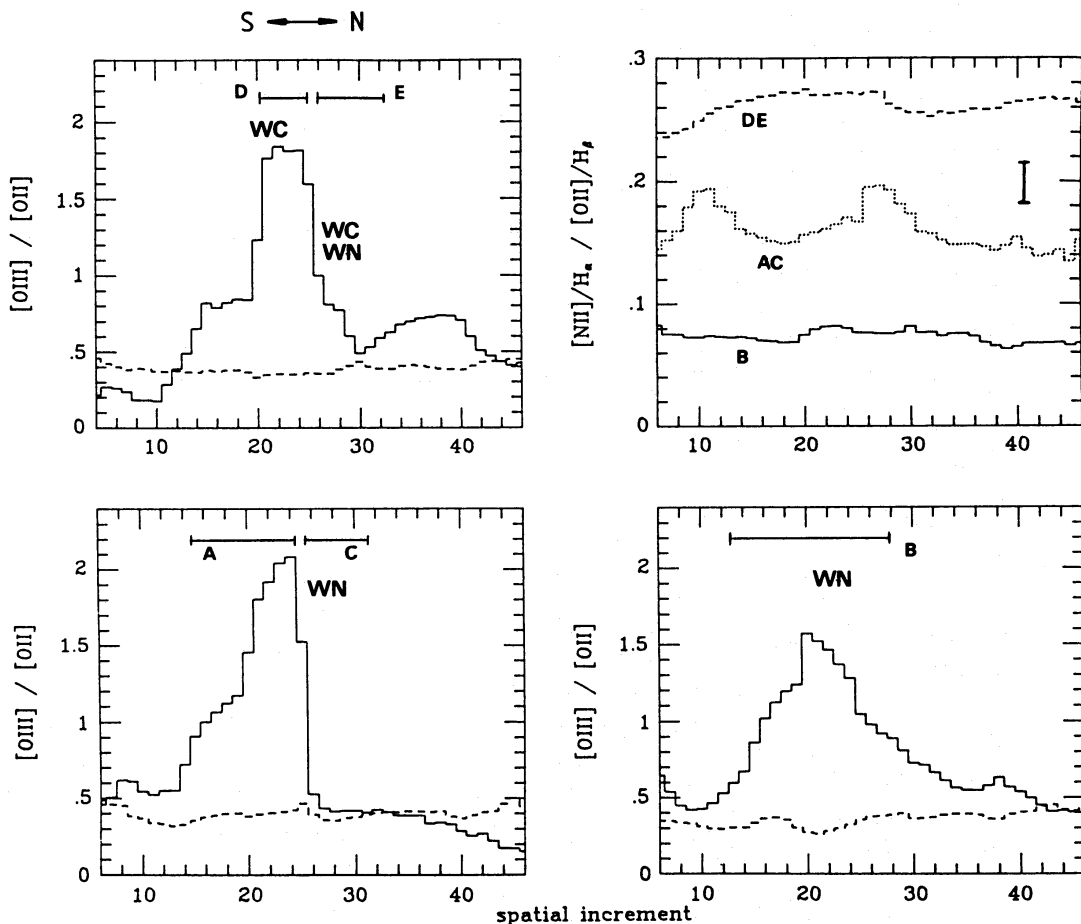


Figure 5. Spatial profiles of $[O\ III]/[O\ II]$ and $([N\ II]/H\alpha)/([O\ II]/H\beta)$ along the slit for each position as shown in Fig. 1. The profiles have been smoothed by a Gaussian of $\sigma=2$ spatial increments. In the $[O\ III]/[O\ II]$ plots, the short dashed line shows the ratio of $H\alpha/H\beta$ divided by 10. In the upper right plot each profile is displaced from the one below by adding a constant value of 0.1.

AC. Therefore the overall picture indicates that the regions containing the bulk of the O^{++} are not very extended and are preferentially located to the south of the core of the $H\ II$ complex, where the observed continua are weaker. The reduced extension of the $[O\ III]$ implies that the He^{++} zone, if at all present, needs to be very small, if the traditional ionization structure geometry is assumed. Therefore the $He\ II$ lines observed in some positions in the nebula must be essentially of stellar origin.

The ratio $([N\ II]/H\alpha)/([O\ II]/H\beta)$ is fairly constant across every position in the nebula, except perhaps across position A, where the spatial distribution is less uniform presenting two maxima 30 per cent over the mean value. This ratio is not highly affected by reddening, unless this is very large, and at any rate, as mentioned above, the reddening seems to be very uniform across the entire nebula. The constancy of the $([N\ II]/H\alpha)/([O\ II]/H\beta)$ ratio seems to indicate that it is not a sensitive function of the excitation, which shows large variations over the nebula; therefore it can be considered as a good indicator of the N/O abundance ratio. The peaks found are very confined spatially and seem to coincide, in the case of C, with the presence of WR features. They could then represent real enhancements of the N/O ratio although we consider this evidence to be marginal.

Point-to-point diagrams of the behaviour of the line ratios $[N\ II]\ \lambda 6584/[S\ II]\ \lambda\lambda 6717, 6731, ([O\ II]+[O\ III])/H\beta$ (Pagel *et al.* 1978) and the composite line ratio $([O\ II]/H\beta) \times ([O\ II]/[S\ II])$

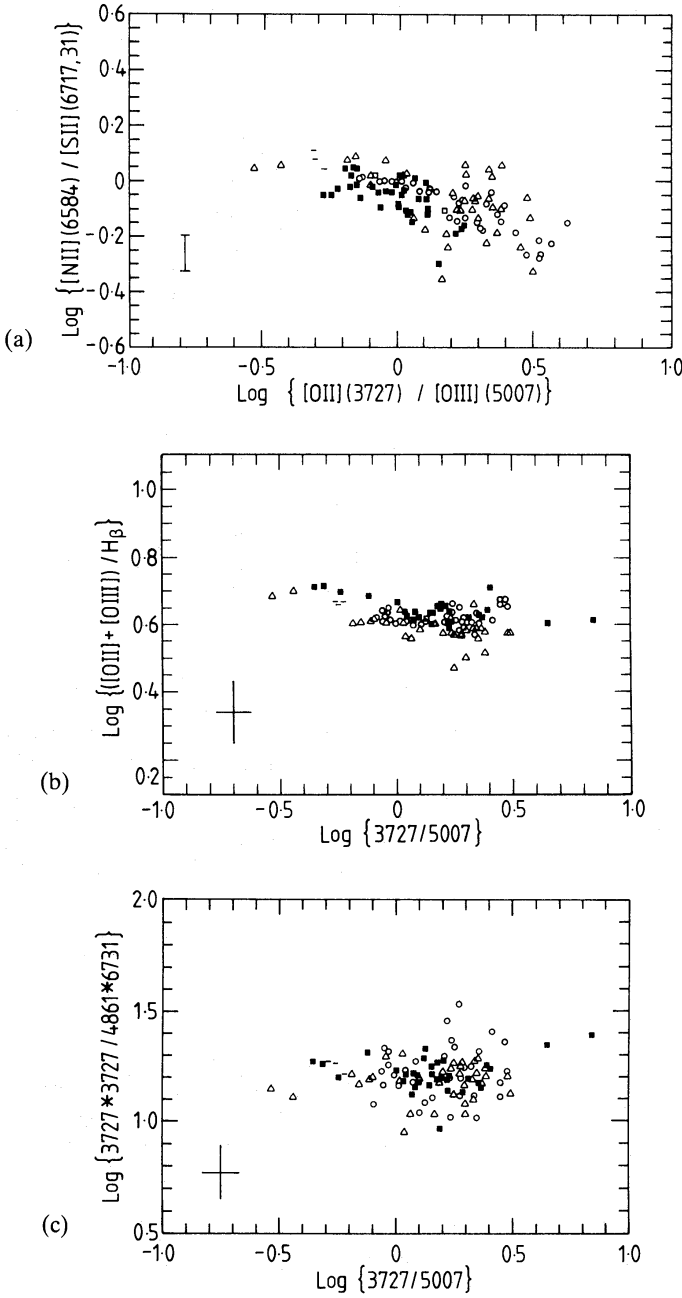


Figure 6. Point-to-point variations of the line ratios (a) $[\text{NII}]/[\text{SII}]$, (b) $([\text{OII}] + [\text{OIII}])/\text{H}\beta$ and (c) $([\text{OII}]/\text{H}\beta) \times ([\text{OII}]/[\text{SII}])$, versus the excitation measured as $[\text{OII}]/[\text{OIII}]$. Each point represents a spatial increment; ○: slit position B, △: AC and ■: DE.

(Evans & Dopita 1985) as a function of the degree of excitation measured by $[\text{OII}]/[\text{OIII}]$ are shown in Fig. 6. For each spatial increment chosen, the accuracy of the ratios is typically better than 10 per cent. Despite the large range of values for the excitation, most of the selected line ratios remain substantially uniform, implying that any one of them can be used to describe the H II region as a whole.

The relative decrease of $[\text{NII}]/[\text{SII}]$ with $[\text{OII}]/[\text{OIII}]$ seen in Fig. 6(a), can be understood as an excitation effect due to the lower ionization potential of S^+ with respect to N^+ combined with the relatively low S^+/S^{++} ratio. A similar effect has been reported by McCall *et al.* (1985) for several H II regions in M101 located at constant radius, and hence probably sharing the same abundance.

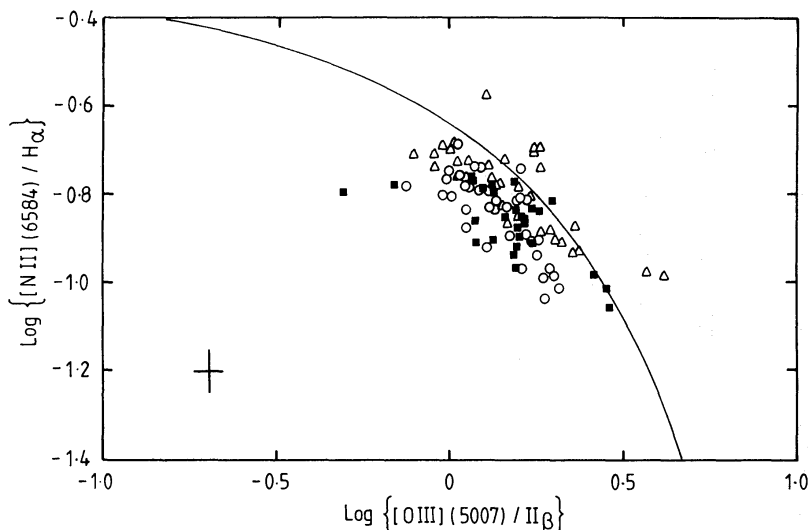


Figure 7. Point-to-point variations in the line ratios $[\text{N II}] \lambda 6584/\text{H}\alpha$ and $[\text{O III}] \lambda 5007/\text{H}\beta$. The continuous curve is the corresponding relation for different H II regions after Baldwin *et al.* (1981).

Fig. 7 shows a plot of $[\text{N II}]/\text{H}\alpha$ against $[\text{O III}]/\text{H}\beta$, analogous to one of the diagnostic plots of Baldwin, Phillips & Terlevich (1981), whose average relationship for the integrated spectra of different H II regions is also shown. There is a striking similarity between the effects of ionization parameter on different portions of NGC 604 (where all other relevant quantities are presumably constant) and those of the combination of chemical composition, stellar effective temperature and possibly ionization parameter as well (*cf.* Evans & Dopita 1985) on the global spectra of giant H II regions.

5.2 ABUNDANCES

The large extension of NGC 604, and the existing strong differences in excitation that we have discussed before, imply that different observations over the nebula could provide fairly different values of ionic abundances while the corresponding total abundances could be more or less the same.

Ionic and total abundances taken from the literature have been recalculated with the same algorithm used for the present observations and are given in Table 4.

5.2.1 Oxygen

Our results for oxygen are in agreement with those derived from the work of Peimbert (1970, P70) and Smith (1975, S75), using their $[\text{O III}]$ temperatures for both ions. For the data of Kwitter & Aller (1981, KA81) a lower value of the total oxygen abundance would be obtained ($12 + \log \text{O}/\text{H} = 8.09$) if their $[\text{O III}]$ temperature were used for all the ions; however, this discrepancy is eliminated when using their proposed $t[\text{O II}]$ in calculating the O abundance. It is also possible, as suggested by Wooden (1984, unpublished work), that KA81 observed a region in the faint north halo of the H II complex very distant from the core.

For two regions, E and A, we obtain a total oxygen abundance lower and higher respectively than average. In the case of region E, the temperature derived from the observed $[\text{O III}]$ ratio and the predicted $[\text{O II}]$ line temperature from S80 give the same value of 10 000 K; therefore a

one-zone temperature scheme was adopted in the calculations. However, the derived [S III] temperature is lower. That might suggest the presence of a small-scale temperature fluctuation, in which case the O/H abundance would be underestimated in this region. No differences in temperature seem to exist in region A and, although the difference in abundance is not large compared with the errors (typically 0.1 dex), in this case it might represent a real enhancement in the oxygen abundance to the south-east of the nebula. A supernova remnant was discovered by Benvenuti, D'Odorico & Dumontel (1979) near this region. If it has caused local contamination, we would expect the ratios O/Ne, O/S, O/Ar to be unchanged and O/N to be enhanced (see Rosa & Mathis 1985). Of these effects, only the constancy of O/Ne applies, so that the case for such an effect is marginal at best.

5.2.2 Helium

The He⁺ abundances deduced in the present work are between the values of KA81 and those of Peimbert & Spinrad (1970, PS70) if the abnormally high value for the He I $\lambda 5876$ Å flux in region E is not considered. This line is possibly contaminated by adjacent stellar He I emission presenting a broad base and wings with a non-negligible flux contribution.

Contrary to what is found in the literature, the computed ICFs required for the calculation of the total He abundance are not very high (see Table 4), except for position E where the deduced ICF is undefined, as mentioned at the end of Section 4.4.2. This is expected on the basis of the effective temperatures estimated for the ionizing stars in NGC 604.

Although our He⁺/H⁺ values are not far from those found in the literature (see Table 4), the total helium abundances we deduce are substantially lower due to the different ICFs used. The mean value for He/H, excluding region E, is 0.088 ± 0.006 . Some helium enrichment might be possible for region E whose ionic abundance He⁺/H⁺ is already higher than average. Strong features of WR stars are observed at this position and some helium enrichment could result as a consequence of the strong mass loss expected from a cluster with a large number of WR stars (Conti & Massey 1981; Rosa & D'Odorico 1982). Theoretical models by Maeder (1981) predict that at the WN stage, a considerable amount of the mass lost by a WR star is in the form of ⁴He. This enrichment, if real, represents just a local enhancement. It might then be advisable to observe more than one position in a nebula if good He abundance determinations are wanted. Our mean value for the total He yields a value of Y, He abundance by mass, of $Y = 0.260 \pm 0.013$, fitting well the relation between Y and O abundance obtained by Pagel, Terlevich & Melnick (1986) for H II galaxies.

5.2.3 Sulphur

In the case of sulphur, our S⁺/H⁺ agrees with the results found in the literature (see Table 4 and Hawley & Grandi 1977, HG77). Data on S⁺⁺/H⁺ were determined by KA81 from observations of the [S III] $\lambda 6312$ Å line and by HG77 from observations of the [S III] $\lambda\lambda 9532, 9069$ Å lines. In both cases sulphur is found to be predominantly present as S⁺⁺ which is about an order of magnitude more abundant than S⁺, although the actual values of $12 + \log(S^{++}/H^+)$ are somewhat discrepant (6.58 and 7.04, respectively). Our S⁺⁺ abundances are about twice those of KA81 but agree with those of HG77, though their observations cover the whole central region. Our total S abundances are, however, lower than theirs because we disagree with the large allowance they made for the presence of S³⁺ (Dennefeld & Stasinska 1983). Our calculated mean ionic abundances give $\log(O/S) = 1.6$ which is essentially the same as the one derived for the Orion Nebula by Peimbert & Torres-Peimbert (1977).

5.2.4 Nitrogen

The N/O ratios found for every position observed are similar to one another, contrary to what is found by Skillman (1985) for NGC 5471, and the mean value is consistent with the values obtained by KA81 and S75. As discussed before, the $[\text{N II}]/[\text{O II}]$ ratio is found to be a very good abundance indicator.*

6 Conclusions

Combined spectrophotometry using the IPCS and CCD detectors has been obtained of the GEHR NGC 604 in M33, covering the wavelength range from 3500 \AA – $1 \mu\text{m}$, in order to investigate any possible abundance inhomogeneities through the nebula and to check the consistency of abundances derived by standard methods in parts of it where the ionization differs by large factors.

Spectral features characteristic of WR stars are clearly detected in three of the observed positions in agreement with previous observations by other investigators. However, the reddening is found to be remarkably constant across the entire nebula, implying that the obscuring material is uniformly distributed and suggesting that no association between dust and WR clusters exists.

The excitation is seen to change considerably across the nebula with the most excited regions always to the south. Yet the line-intensity ratios $[\text{N II}]/[\text{S II}]$, $([\text{O II}]+[\text{O III}])/H\beta$ and $([\text{O II}]/H\beta) \times ([\text{O II}]/[\text{S II}])$ remain substantially constant; they therefore can be used as parameters characterizing the H II region as a whole and as potential abundance indicators. The ratio $([\text{N II}]/H\alpha)/([\text{O II}]/H\beta)$ is also fairly constant over the nebula and it can be considered to be a good indicator of the N/O abundance ratio.

No substantial abundance differences are found across the nebula. Despite the large range of excitation seen, the O/H abundance seems to be rather constant with a mean value of $12+\log(\text{O}/\text{H})=8.40$ which agrees well with previous values found in the literature. Sulphur is found to be predominantly in the form of S^{++} and the total S abundance is the same as that derived for the Orion nebula (Peimbert & Torres-Peimbert 1977).

Helium abundances have been obtained using as many helium lines as possible. The factors needed to correct for the presence of neutral helium have been determined using a new parameter, $\eta=(\text{O}^+/\text{O}^{++})/(\text{S}^+/\text{S}^{++})$, which is intrinsically linked to the ‘ionization temperature’ (the formal effective temperature of the ionizing cluster) and weakly sensitive to the ionization parameter or the electron temperature. Except for one position in the nebula where the ICF cannot be determined and some local helium enrichment could be present, moderate values of the ICFs are found, leading to values of He/H substantially lower than those previously reported. The mean value of He/H yields a value of Y , He abundance by mass, of $Y=0.260\pm0.013$ which fits the relation between Y and Z (metallicity) recently obtained by Pagel *et al.* (1986).

Acknowledgments

The INT is operated on the island of La Palma by the RGO at the Observatorio del Roque de los Muchachos of the Instituto de Astrofísica de Canarias. I. R. G. Wilson gave invaluable support during observations. We also thank the staff of the La Palma Operations Division and P. Gómez and A. Mampaso for their help. It is a pleasure to thank Max Pettini, Michael Rosa and Evan Skillman for their careful reading of the manuscript and sensible suggestions.

*It has recently been suggested (Rubin 1986) that dielectronic recombination of O^{++} to O^+ should be taken into account when calculating the N/O ratio using the familiar optical lines. From Rubin’s calculations it follows that $r([\text{O II}])$ needs to be revised slightly downwards, but the N/O ratio is not greatly affected.

Elena Terlevich and Pepe Vilchez enjoyed the hospitality of the RGO during the realization of this work. Angeles Díaz acknowledges the grant of a Henri-Chretien Award by the AAS.

References

- Aller, L. H., 1984. *Physics of Thermal Gaseous Nebulae*, Reidel, Dordrecht, Holland.
- Baldwin, J. A., Phillips, M. M. & Terlevich, R., 1981. *Publs astr Soc. Pacif.*, **93**, 5.
- Barker, T., 1978. *Astrophys. J.*, **221**, 145.
- Benvenuti, P., D'Odorico, S. & Dumontel, M., 1979. *Astrophys. Space Sci.*, **66**, 39.
- Brocklehurst, M., 1971. *Mon. Not. R. astr. Soc.*, **153**, 471.
- Conti, P. S. & Massey, P., 1981. *Astrophys. J.*, **249**, 471.
- Dennefeld, M. & Stasinska, G., 1983. *Astr. Astrophys.*, **118**, 234.
- de Vaucouleurs, G. & de Vaucouleurs, A., 1971. *Astrophys. Lett.*, **8**, 17.
- Díaz, A. I., Pagel, B. E. J. & Wilson, I. R. G., 1985. *Mon. Not. R. astr. Soc.*, **212**, 737.
- Dinerstein, H. L., 1980. *Astrophys. J.*, **237**, 486.
- Dinerstein, H. L. & Shields, G. A., 1986. *Astrophys. J.*, **311**, 45.
- D'Odorico, S., Rosa, M. & Wampler, E. J., 1983. *Astr. Astrophys. Suppl. Ser.*, **53**, 97.
- Evans, I. N. & Dopita, M. A., 1985. *Astrophys. J. Suppl.*, **58**, 125.
- Garnett, D. A. & Shields, G. A., 1986. *Astrophys. J.*, submitted.
- Hawley, S. A. & Grandi, S. A., 1977. *Astrophys. J.*, **217**, 420.
- Hayes, D. S., 1970. *Astrophys. J.*, **159**, 165.
- Israel, F. P. & van der Kruit, P. C., 1974. *Astr. Astrophys.*, **32**, 363.
- Kurucz, R. L., 1979. *Astrophys. J. Suppl.*, **40**, 1.
- Kwitter, K. B. & Aller, L. H., 1981. *Mon. Not. R. astr. Soc.*, **195**, 939.
- Lequeux, J., Peimbert, M., Rayo, A., Serrano, A. & Torres-Peimbert, S., 1979. *Astr. Astrophys.*, **80**, 155.
- McCall, M. L., Rybski, P. M. & Shields, G. A., 1985. *Astrophys. J. Suppl.*, **57**, 1.
- Maeder, A., 1981. *Astr. Astrophys.*, **99**, 97.
- Mathis, J. S., 1982. *Astrophys. J.*, **261**, 195.
- Mathis, J. S., 1985. *Astrophys. J.*, **291**, 247.
- Mathis, J. S., Chu, Y.-H. & Peterson, D. E., 1985. *Astrophys. J.*, **292**, 155.
- Melnick, J., 1979. *Astrophys. J.*, **228**, 112.
- Mendoza, C., 1983. In: *Planetary Nebulae, IAU Symp. No. 193*, p. 143, ed. Flower, D. R., Reidel, Dordrecht, Holland.
- Mihalas, D., 1972. *Non-LTE Model Atmospheres for B and O Stars*, NCAR-TN/STR-76.
- Oke, J. B., 1974. *Astrophys. J. Suppl.*, **27**, 21.
- Pagel, B. E. J., 1978. *Mon. Not. R. astr. Soc.*, **183**, 1.
- Pagel, B. E. J., Terlevich, R. & Melnick, J., 1986. *Publs astr. Soc. Pacif.*, **98**, 1005.
- Pagel, B. E. J., Edmunds, M. G., Fosbury, R. A. E. & Webster, B. L., 1978. *Mon. Not. R. astr. Soc.*, **184**, 569.
- Peimbert, M., 1970. *Publs astr. Soc. Pacif.*, **82**, 636.
- Peimbert, M. & Costero, R., 1969. *Bols. Obs. Ton. y Tacubaya*, **5**, 3.
- Peimbert, M. & Spinrad, H., 1970. *Astrophys. J.*, **159**, 809.
- Peimbert, M., Rodríguez, L. F. & Torres-Peimbert, S., 1974. *Rev. Mex. Astr. Astrofis.*, **1**, 129.
- Peimbert, M. & Torres-Peimbert, S., 1977. *Mon. Not. R. astr. Soc.*, **179**, 217.
- Rosa, M., 1982. *PhD thesis*, University of Heidelberg.
- Rosa, M. & D'Odorico, S., 1982. *Astr. Astrophys.*, **108**, 339.
- Rosa, M. & Mathis, J. S., 1985. In: *ESO Workshop Production and Distribution of the CNO Elements*, p. 207, eds Danziger, I. J., Matteucci, F. & Kjær, K.
- Rosa, M. & Solf, J., 1984. *Astr. Astrophys.*, **130**, 29.
- Rubin, R. H., 1986. *Astrophys. J.*, **309**, 334.
- Seaton, M. J., 1975. *Mon. Not. R. astr. Soc.*, **170**, 475.
- Skillman, E. D., 1985. *Astrophys. J.*, **290**, 449.
- Smith, H. E., 1975. *Astrophys. J.*, **199**, 591.
- Stasinska, G., 1980. *Astr. Astrophys.*, **84**, 320.
- Stasinska, G., 1982. *Astr. Astrophys. Suppl. Ser.*, **48**, 299.
- Stone, R. P. S., 1977. *Astrophys. J.*, **218**, 767.
- Terlevich, R. & Melnick, J., 1981. *Mon. Not. R. astr. Soc.*, **195**, 839.
- Whitford, A. E., 1958. *Astr. J.*, **63**, 210.